JACS
JOURNAL OF THE AMERICAN CHEMICAL SOCIETY
Article
pubs.acs.org/JACS

Simulation of Metal–Ligand Self-Assembly into Spherical Complex M_6L_8

Makoto Yoneya,*[,†] Tomohiko Yamaguchi,[†] Sota Sato,[‡] and Makoto Fujita[‡]

[†]Nanosystem Research Institute, National Institute of Advanced Industrial Science and Technology, 1-1-1 Umezono, Tsukuba 305-8568, Japan

[‡]Department of Applied Chemistry, School of Engineering, University of Tokyo, 7-3-1 Hongo, Bunkyo-ku, Tokyo, 111-8656, Japan

Supporting Information

ABSTRACT: Molecular dynamics simulations were performed to study the self-assembly of a spherical complex through metal–ligand coordination interactions. M_6L_8, a nanosphere with six palladium ions and eight pyridine-capped tridentate ligands, was selected as a target system. We successfully observed the spontaneous formation of spherical shaped M_6L_8 cages over the course of our simulations, starting from random initial placement of the metals and ligands. To simulate spontaneous coordination bond formations and breaks, the cationic dummy atom method was employed to model nonbonded metal–ligand interactions. A coarse-grained solvent model was used to fill the gap between the time scale of the supramolecular self-assembly and that accessible by common molecular dynamics simulation. The simulated formation process occurred in the distinct three-stage (assembly, evolution, fixation) process that is well correlated with the experimental results. We found that the difference of the lifetime (or the ligand exchange rate) between the smaller-sized incomplete clusters and the completed M_6L_8 nanospheres is crucially important in their supramolecular self-assembly.

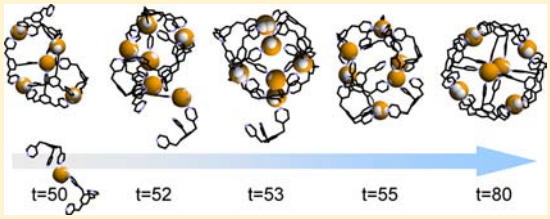

INTRODUCTION

Over the past decade, extensive studies have been done on coordination cages that are formed by the complexation of transition-metal ions with exomultidentate ligands.[1,2] For example, 12 palladium ions (M) and 24 pyridine-capped banana-shaped ligands (L) are reported to self-assemble into a coordinated nanosphere ($M_{12}L_{24}$) in polar solvents.[3] These nanospheres could be used as functional molecular capsule materials.[4] Moreover, this $M_{12}L_{24}$ nanosphere further self-assembles into monolayered hollow, spherical, vesicle-like structures.[5] Such self-assembly of many subunits into a giant supramolecule can be a model system to study complex self-organizations in nature, for example, the capsids of spherical viruses consist of 60 T (T is called the triangulation number) identical protein subunits.[6] The capsid is the protein coat encasing the viral genome, and its near-spherical shape (with icosahedral symmetry) is important because it provides a maximal cavity for a given surface area. In both the spherical complex and the viral capsid systems, their formations are self-limiting, which is significantly different than the self-assembly of crystals that can, in principle, grow without limits.[7] Understanding the mechanism of this supramolecular self-assembly is crucially important for designing bioinspired nanosphere materials.

Motivated by the inherent difficulty of direct visualization of evolving capsid assemblies, molecular dynamics (MD) simulations have been applied.[7−11] In these simulations, individual protein subunits and the interactions between them are highly simplified in various fashions. Compared to the viral capsid systems, the spherical complex systems are composed of far simpler molecules and facilitate more direct modeling. This may contribute to a reduction in the ambiguity that arises from a wide range of possible modeling strategies. Despite this advantage, MD simulation has not been applied to the spherical complex assembly to the best of our knowledge. In this study, we report the first MD application to this problem.

Herein, we focus on one of the simplest examples of the spherical complex, M_6L_8, a nanosphere of octahedral symmetry with six palladium (Pd) ions and eight tridentate ligands (ligand **1** in Figure 1).[12] The M_6L_8 complex can be readily formed from a 4:3 mixture of ligand **1** and $Pd(NO_3)_2$ in dimethyl sulfoxide (DMSO) at 90 °C. The formation process was directly monitored by nuclear magnetic resonance spectroscopy in

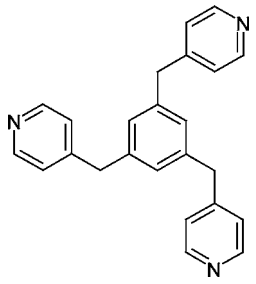

Figure 1. Pyridine-capped tridentate ligand **1**.

Received: April 13, 2012
Published: August 13, 2012

   dx.doi.org/10.1021/ja303542r | J. Am. Chem. Soc. 2012, 134, 14401−14407

DMSO-d_6 solvent, which shows the completed complexation reaction within 5 min.[12] Additionally, no peaks other than those due to the M_6L_8 complex were observed, which establishes the monodisperse assembly and remarkable thermodynamic stability of the complex. The structure of M_6L_8 was determined by X-ray diffraction (XRD),[12] which reveals that the six Pd(II) occupy the apexes of the octahedral array and that the trigonal faces of the octahedron are capped by the tripodal nonplanar ligand **1** in a truncated fashion, leading to a near-spherical shape.

Even in this simple case, the self-assembly time scale would be far beyond the accessible time scale of common MD simulations. We therefore need to speed it up to fill the gap between the simulations and the real reaction systems. By applying the coarse-grained solvent model that is described in the next section, Model and Methods, we succeeded in observing a spontaneous formation of the spherical-shaped M_6L_8 cages over the course of the simulations, which were started from random initial placement of the metals and ligands.

MODEL AND METHODS

First, the metal−ligand coordination interaction was modeled. Various methods have been proposed to model the coordination of metal ions and ligands.[13] For example, the bonded model uses covalent bonds between metal ions and coordinating sites of ligands to maintain the specific symmetry of the coordinations. For our purposes, this bonded model did not apply because we wanted to simulate spontaneous coordination bond formations and breaks over the course of the simulations. In this case, we applied a nonbonded model that maintains the coordination with the electrostatic and van der Waals interactions. More specifically, we applied the cationic dummy atom (CaDA) model, which has previously been applied to zinc complex proteins.[14] The zinc CaDA model uses four identical dummy atoms that are tetrahedrally attached to the zinc ions and transfers the atomic charge of the zinc divalent cation evenly to the four dummy atoms. Akin to this zinc model, the Pd(II) CaDA model uses four identical dummy atoms coplanarly attached to the Pd, as shown in Figure 2. The Pd−dummy distance was defined (as 0.09 nm) to reproduce the averaged Pd−N distance from the XRD study[12] (full detail of the Pd(II) CaDA model can be found in a Supporting Information). The metal−ligand binding in the Pd(II) CaDA model is purely electrostatic and too simple to represent the real coordination interaction. However, we applied this simple CaDA approach, since we aimed to propose the minimum model for the M_6L_8 self-assembly.

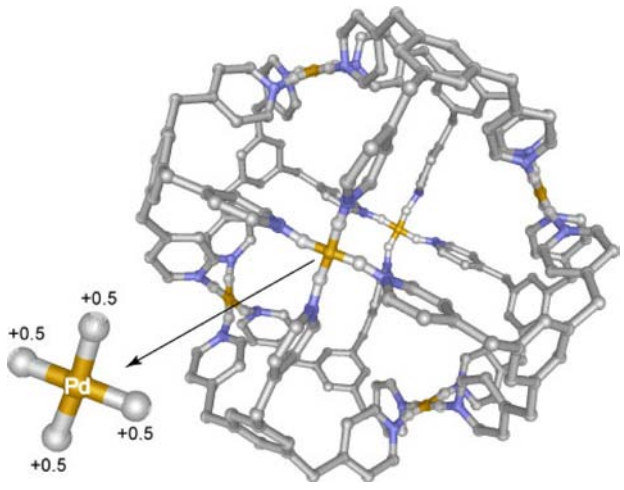

Figure 2. Pd(II) model using CaDA and M_6L_8 nanosphere. The Pd(II) CaDA model uses four identical dummy atoms that are coplanarly attached to the Pd ions and transfers the atomic charge of the Pd(II) cation evenly to the four dummy atoms.

For ligand **1**, we applied the flexible united-atom model with the exception that all of the bond-stretching degrees of freedom were constrained to the equilibrium bond lengths. For the inter- and intramolecular interactions, a general AMBER force field[15] was used in combination with CH and CH_2 united-atom parameters from a reoptimized united-atom force field.[16] Some torsional potentials related to the united atoms that maintain the tripodal nonplanar shape of ligand **1** were assigned to the rather high potential barrier ones in the AMBER improper torsional potentials. This is because we found that the flexibility of this tripodal shape interferes with (slows down) the formation of the M_6L_8 nanosphere. Restrained electrostatic potential (RESP) charges,[17] obtained using *ab initio* molecular orbital calculations with the B3LYP/6-31G(d) level in the Gaussian03 program,[18] were used for the atomic charges of the ligand.

Next, we will explain the method we used to speed up the assembly process of the model metal−ligand system in solution. As in the Introduction, we must introduce the methods used to accelerate the assembly process to fill the time scale gap between the real and simulated systems. In this study, we accelerate assembly of metals and ligands by treating the solvent implicitly as a continuum medium. There are various kinds of implicit solvent models.[19] Here, we apply a combination of three methods, i.e., Langevin (stochastic) dynamics, reaction fields, and coarse-grained potentials. To account for the dynamic effects of the solvent molecules, Langevin dynamics (LD),[20] which adds a friction and random force to the conventional MD, was applied. To represent the electrostatic effects of the solvent, the generalized reaction field method,[21] which extends the "classical" reaction field method to ionic systems, was used. In this method, the relative dielectric constant beyond the distance parameter for the complete neutralization (screening) can be separately specified as the far-field value ε_{rf} from the near-field value ε_r. Similar to the electrostatic effects, van der Waals interactions between the ligands are also screened by the solvation to effectively be short-range repulsive ones. We apply a Weeks−Chandler−Andersen (WCA) potential[22] for this short-range repulsive potential. The WCA potential truncates at the repulsive part of the common Lennard-Jones potential and shifted as follows:

$$V(r_{ij}) = \begin{cases} 4\varepsilon_{ij}\left[\left(\frac{\sigma_{ij}}{r_{ij}}\right)^{12} - \left(\frac{\sigma_{ij}}{r_{ij}}\right)^{6}\right] + \varepsilon_{ij} & r_{ij} < 2^{1/6}\sigma_{ij} \\ 0 & r_{ij} \geq 2^{1/6}\sigma_{ij} \end{cases} \quad (1)$$

where r_{ij} is the distance between the atoms and ε and σ are Lennard-Jones potential parameters. Such combinations of the Coulomb interaction with an effective dielectric constant and the WCA potential interaction are used as a simple implicit solvent model in the ionic system study.[23] AMBER[15,16] values were used for ε and σ in the ligand model. For Pd atoms, these parameters were taken from the literature.[24]

To realize the M_6L_8 self-assembly within the available computational time, we should enhance the probability of coordination formation between the Pd(II) ions and the ligands. Inclusion of the nitrate (NO_3^-) counterions reduces this probability since these would compete with the ligands for the Pd(II) ions. Then we first modeled the system without the nitrate ions to enhance the probability and then to accelerate the simulated self-assembly. We will show the results with including the nitrate ions in the later section. Without the nitrate ions, charge neutrality of the simulation system is not fulfilled. For this reason, we did not apply Ewald-like methods that usually require charge neutrality of the system but applied the generalized reaction field method.

Trajectories were produced using the MD program package GROMACS (version 4.0.7)[25] with modification of the nonbonded interaction routine to employ the WCA potential described above. LD time integration was done with the leapfrog stochastic dynamics integrator[26] and LINCS bond constraint[27] with the time step of 5 fs.

dx.doi.org/10.1021/ja303542r | J. Am. Chem. Soc. 2012, 134, 14401−14407

Charge group-based twin-range 0.65 nm van der Waals and 1.4 nm electrostatic cutoff distances[28] were applied to nonbonded interactions. In contrast to the common setting for the latter value (1.4 nm),[29] the former value (0.65 nm) is rather short compared to the common one because we utilized the short-ranged WCA potential. The far-field relative dielectric constant in the generalized reaction field method, ε_{rf}, was specified as 47.0 for the DMSO solvent setting.[29] The simulation temperature was maintained by coupling to a stochastic thermostat with a time constant τ_t = 0.1 ps via LD. The LD friction coefficient for each atom is specified as the GROMACS default value, i.e., mass/τ_t.

The GROMACS molecular topology file for the ligand **1** and CaDA Pd(II) models with the atomic charge assignments that help reproduce the simulation in this study are found in the Supporting Information. The topology file for ligand **1** was created with the help of the program "acpype"[30] as the interface to the automatic atom-type bond-type perception program "antechamber"[31] and then modified to use the CH and CH_2 united atoms.

By using the models and methods described above, we checked the thermodynamic stability of the M_6L_8 structure obtained from the XRD study.[12] We were convinced that the coordinated nanosphere was kept stable at the experimental temperature of 90 °C with our simulation model (as the snapshot after the 10 ns LD run shows in Figure 2).

RESULTS AND DISCUSSION

We first tried a relatively small system to clarify the acceleration factors in the MD simulation, using the model in the previous section. The initial structure was made by random placement of 24 Pd(II) and 48 ligand **1** models (which corresponds to four M_6L_8 nanospheres) in the cubic simulation box with a volume of $(20\ \text{nm})^3$, as shown in Figure 3. The initial concentration is

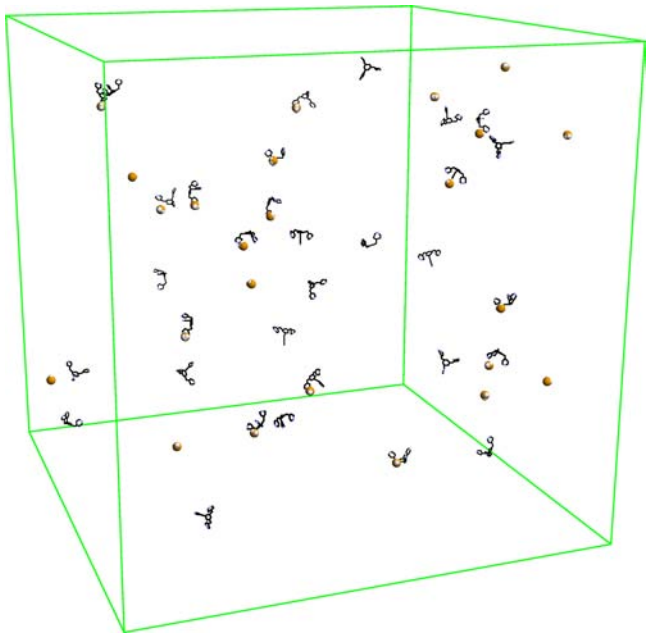

Figure 3. Initial structure made by random placement of 24 Pd(II) and 48 ligand **1** models (which corresponds to four M_6L_8 nanospheres) in the cubic simulation box with a volume of $(20\ \text{nm})^3$.

the factor that affects the formation process of the M_6L_8 nanosphere, i.e., a long time free diffusion occurred when the initial concentration was too low, and a highly random aggregation occurred when it was for too high. The concentration of the Pd(II) ions and ligands in the initial structure described above was chosen by trial and error and is about 1/234 of that in the M_6L_8 crystal state,[12] but a far higher concentration than that of the experimentally prepared solution (0.01 mol/L).

There are many other factors that could affect the formation rate of the spherical complex. As previously mentioned, the conformational rigidity of the ligand's tripodal shape is one factor. Temperature is surely another factor, but we set it to the experimental condition, i.e., 90 °C (363 K). Herein, we focus on the parameter that controls the metal−ligand coordination interactions, i.e., the near-field relative dielectric constant ε_I. The far-field relative dielectric constant, ε_{rf}, was specified as 47.0 for the DMSO solvent, as described in the previous section. Application of this value (ε_r = 47) for even short distance (near-field) charge−charge interactions is clearly inadequate because this means there is as many DMSO molecules (as like continuum medium) between these short distance separated charges. However, common choice for the near-field ε_r = 1, which corresponds to the vacuum, was also inadequate in this study, because this completely neglects pseudoligand effect of the DMSO solvent. A polar solvent, such as DMSO, could behave like a ligand, where the resulting metal−solvent interaction enhances the metal−ligand exchange probability. This pseudoligand effect of the polar solvent could be parametrized as the enlarged ε_r than one that corresponds to the vacuum.

We compare the results with three different near-field dielectric constants, ε_r = 1.0, 2.5 and 4.0, all starting with the same initial configuration. Snapshots after the 250 ns LD runs are shown in Figure 4 for these three ε_r settings. Among these, the complete M_6L_8 nanosphere formation during the same 250 ns LD simulation was only observed with ε_r = 2.5. For all six Pd(II) within this completed nanosphere, time variations of the coordination numbers (judged from the distance between Pd and ligand-nitrogen atoms with the threshold of 0.27 nm)[32] of each Pd(II) are shown in Figure 5. The time evolutions in this figure can be divided into three stages: The period up to 50 ns was characterized in rather monotonic increase of coordination numbers by metal−ligand assembly (an assembly stage). The subsequent period, between 50 and 80 ns, was characterized by frequent coordination exchange via tentative coordination of more than four that evolves from a rather randomly assembled cluster to a near-spherical shape (an evolution stage). In the last period, above 80 ns, the coordination numbers were almost fixed to four, and the nanosphere was stable (a fixation stage). These simulated three-stage process in Figure 5 corresponds well to the stages explained in the experimental study.[33]

We then compare the time evolutions of the ligand exchange rates of the three cases, ε_r = 1.0, 2.5, and 4.0. We define the ligand exchange rate as the number of metal−ligand pair alterations over a specified time period, τ (taken here to be 10 ns), and then averaged over all of the pairs in the system. The evaluated rates vs time are shown in Figure 6. In this figure, the broken line corresponds to the exchange rates of the six Pd(II) ions within the completed nanosphere (instead of all the Pd(II) ions) for the LD run with ε_r = 2.5. The broken plot clearly corresponds to Figure 5, i.e., the exchange rate increased in stage 2 (50−80 ns) and then steeply (more than 2 orders of magnitude) decreased to a very small exchange rate value in stage 3 (above 80 ns). We think this large rate difference between the completed nanosphere (in stage 3) and the incomplete clusters (in stage 2) corresponds to the large experimental exchange rate difference between the $M_{12}L_{24}$ nanosphere and a fractional tetramonodentate model complex.[33] The exchange rate constants themselves are much larger

dx.doi.org/10.1021/ja303542r | J. Am. Chem. Soc. 2012, 134, 14401−14407

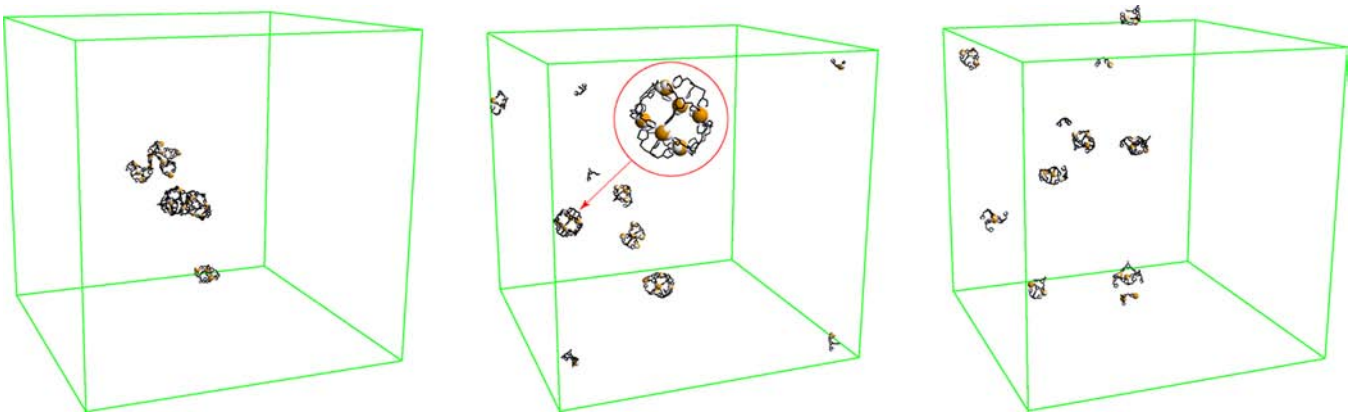

Figure 4. Snapshots after the 250 ns LD runs with setting ε_r = 1.0 (left), 2.5 (center), 4.0 (right). An enlarged image of a completed nanosphere is additionally shown in the central case.

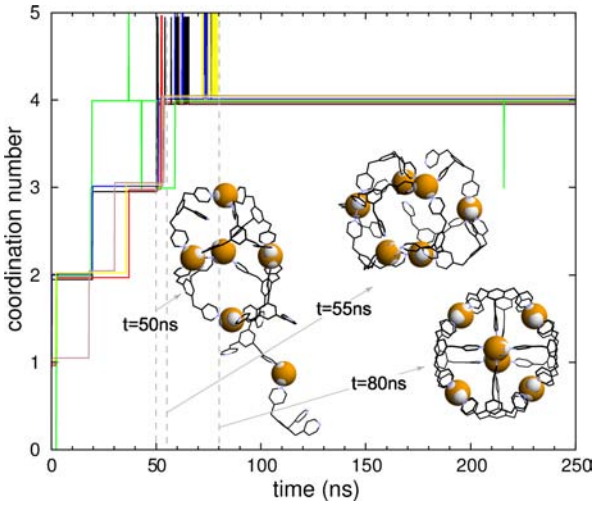

Figure 5. Time variations of the coordination numbers of the six Pd(II) within the completed M_6L_8 nanosphere. Each of the six plots is vertically shifted for clarity. Snapshots at the simulation time of 50, 55, and 80 ns are additionally shown in the figure.

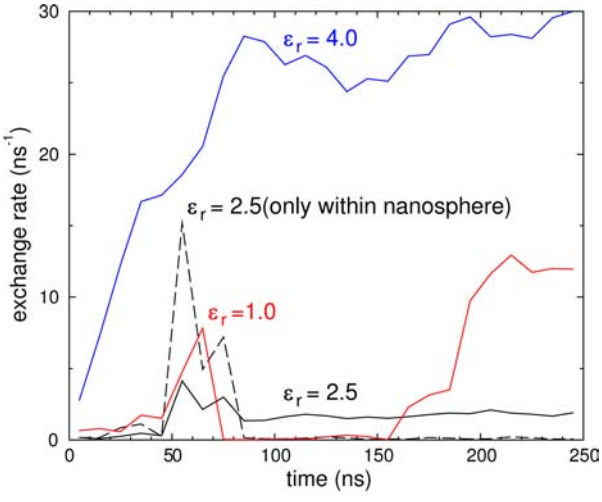

Figure 6. Time variations of the ligand exchange rates for the LD runs with ε_r = 1.0, 2.5, and 4.0. The broken line corresponds to the exchange rates of the six Pd(II) ions within the completed nanosphere (instead of all the Pd(II) ions) for the LD run with ε_r = 2.5.

(ca., 0.1−10 ns^{-1} in Figure 6) in our simulation model than those in experimental report (ranging from ms^{-1} to days^{-1} in ref 33). The real process will depend on both the diffusivity of the fragments in the DMSO solution and the ligand exchange rate. We think the acceleration in our current model was realized by not the fastened diffusivity but the enhanced ligand exchange rates described above. Actually, we found that the diffusion constants in the implicit solvent model with the LD (this study) and those in the explicit DMSO model[34] solvents with the ordinary MD are the same order. Moreover, the dependence of the diffusivity on the simulated self-assembly was diminished in our study because of the much enhanced initial system concentration than that of the real experimental system.

From the results described above, we believe that our accelerated simulation correctly follows the self-assembly process of the real reaction systems when we properly select the simulation parameters, e.g., ε_r. This ε_r can be regarded as a parameter that scales the metal−ligand binding energy, because Coulomb potentials, $q_iq_j/(4\pi\varepsilon r_{ij})$, are the only source of the (metal−ligand) attractive interactions. In the current model, the three state process was seen with ε_r = 2.0−2.5. In contrast, the exchange rate was very large when ε_r = 4.0, and the coordination bonds tend to break before the dimers grow into larger clusters, i.e., clustering rate limiting. When ε_r = 1.0, the Pd(II)−ligand binding energy is relatively strong; thus, it takes a rather long time to break and exchange the coordination bonds to develop new conformers, i.e., breaking rate limiting.

Here, we reconsider the effects of the nitrate counterion inclusion that was discussed in the previous section. For this, we prepared the initial structure with adding 48 nitrate ions at random positions in the structure shown in Figure 3. Fot the nitrate ion model, we applied the model used in Thomas et al. (the parameter set B without polarizability).[35] From this initial structure, we did the corresponding LD run to the case with ε_r = 2.5 in Figure 4. We found that even after a 250 ns LD run, the ligand distribution did not altered much from the initial random one, and no M_6L_8 self-assembly was seen in contrast to the case with ε_r = 2.5 in Figure 4. This occurred because the nitrate ions compete with the ligands for the Pd(II) ions and then interfere with the formation of the M_6L_8 nanosphere, as expected in the previous section's discussions. With regarding the above results and also that there is no strong evidence which shows the active role of the nitrate ions in the M_6L_8 self-assembly process, we

dx.doi.org/10.1021/ja303542r | J. Am. Chem. Soc. 2012, 134, 14401−14407

kept omitting the nitrate counterions from our model in the followings.

Next, we enlarged the system size to see the cluster size distribution during the nanosphere formation. A system eight times larger than the previous one (with 192 Pd ions and 256 ligand models which corresponds to 32 M_6L_8 nanospheres) was made by doubly stacking the MD cells in each of the *X*,*Y*,*Z* directions. A random initial structure was made with a 50 ns high-temperature (473 K) LD run with uncharged Pd(II)−CaDA models (i.e., only repulsive interactions exist within the system). Then the LD run with the original Pd(II)−CaDA model (with the setting $\varepsilon_r = 2.5$) was performed for 1 μs at the temperature of 363 K, as previously used. Cluster size distributions were analyzed based on the ligand−metal coordination bondings from the simulated trajectories.

Figure 7a shows the ligand cluster size distributions as a function of time, where the vertical axis corresponds to the mass fractions. Here, a ligand cluster size of 8 corresponds to the completed M_6L_8 nanosphere, and a size of <8 corresponds to the incomplete ones. As shown in this figure, the distributions equilibrated to the broad peak around cluster size six from the initial 100% monomer distribution. The number of clusters of size 8 (again, corresponds to the completed M_6L_8 nanosphere) were limited to 6, compared to 32 in a perfect assembly. These results imply that the smaller-sized (<8) clusters were not short-lived enough and prevented the formation of complete M_6L_8 nanospheres until monomers are released by the cluster breakup. We should therefore see a much larger difference in the ligand exchange rate (in other words, lifetime) between the smaller-sized clusters and the M_6L_8 nanospheres than appears in the current simulation. In Figure 6, we found that the exchange rates differed by >2 orders of magnitude between the incomplete clusters (in stage 2) and the completed nanosphere (in stage 3). However, the rate difference does not seem to be enough for the monodisperse nanosphere formation. Indeed, a factor of $\sim 10^5$ half-life time (which is inversely proportional to the ligand exchange rate) difference is reported between the fractional model complex and the $M_{12}L_{24}$ nanosphere.[33] A similar large orders of lifetime (exchange rates) difference would then be required between the smaller-sized clusters and the M_6L_8 nanospheres. To confirm this, we did the simulation with forced breakup of the clusters below ligand cluster size six to shorten lifetime of these smaller-sized clusters. The forced breakup was done by switching off the coordination interaction with uncharged Pd(II)−CaDA models for a short period (50 ps) at regular intervals (5 ns). We borrowed this method from the capsid growth study.[7] Resultant time evolution of ligand cluster distributions is shown in Figure 7b. In this simulation, the forced breakup of the smaller-sized clusters was switched on after the time of 0.5 μs. Then, the cluster size distributions were shifted to form the equilibrated peak around eight, the M_6L_8 nanosphere as shown in Figure 7b. In this case, up to 17 M_6L_8 nanospheres were completed after 1 μs LD runs as seen in the final snapshot, as in Figure 8.

The result above shows that we have to incorporate a physical process (instead of the forced breakup in above) to enlarge the lifetime difference. One possible candidate would be the incorporation of an explicit atomistic solvent applied in the capsid growth study.[36] This study reported that the solvent presence aids cluster breakup without subassemblies needing to collide directly. The breakup may help to shorten the lifetime of the smaller-sized imperfect clusters relative to that of the completed nanospheres. Figure 7c shows the corresponding result with the additional incorporation of 96 explicit solvent atoms (with the CH united-atom type) to the first (Figure 7a) case.[37] Completed M_6L_8 nanospheres were increased to 15 from 6 in Figure 7a.

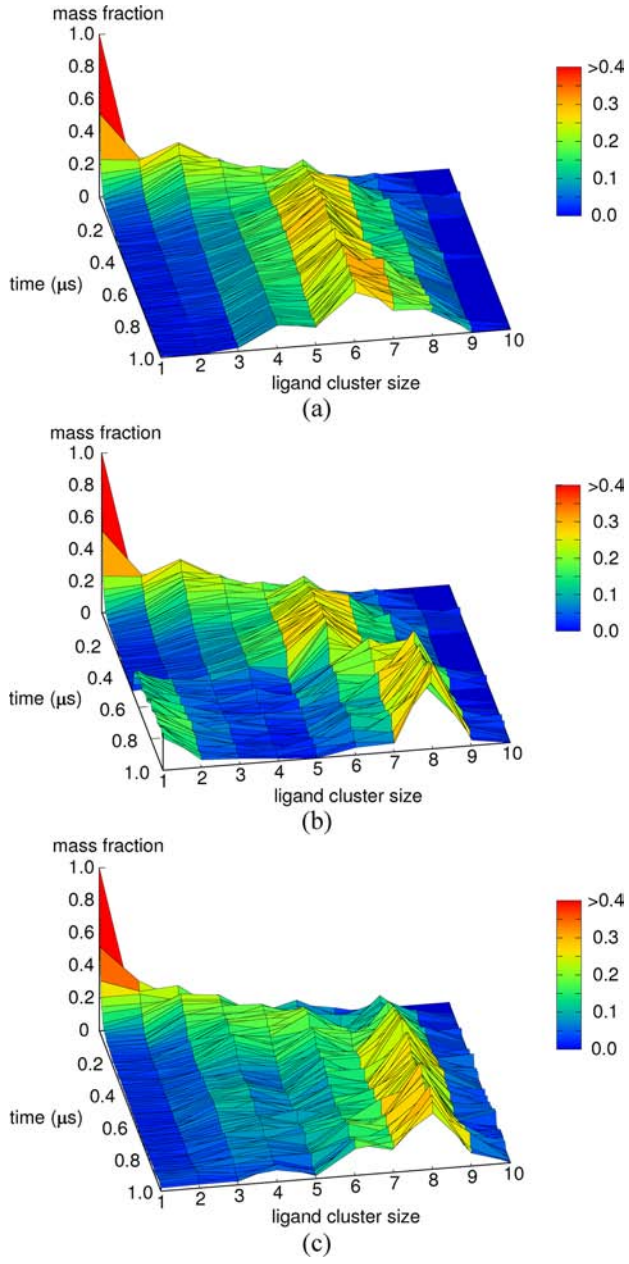

Figure 7. Ligand cluster size distributions as a function of time. The vertical axis corresponds to the mass fractions. (b) In the middle case, the forced breakup of the smaller-sized clusters were switched on after the time of 0.5 μs. (c) In the lower case, an explicit atomistic solvent was additionally incorporated to the first (a) case.

CONCLUSION

We successfully simulated self-assembly of the spherical complex M_6L_8 in the distinct three-stage process that is well correlated with the experimental results.[33] We found that the difference in the lifetimes (or the ligand exchange rates) of the smaller-sized incompleted clusters and the completed M_6L_8 nanospheres is crucially important in this self-assembly.

dx.doi.org/10.1021/ja303542r | J. Am. Chem. Soc. 2012, 134, 14401−14407

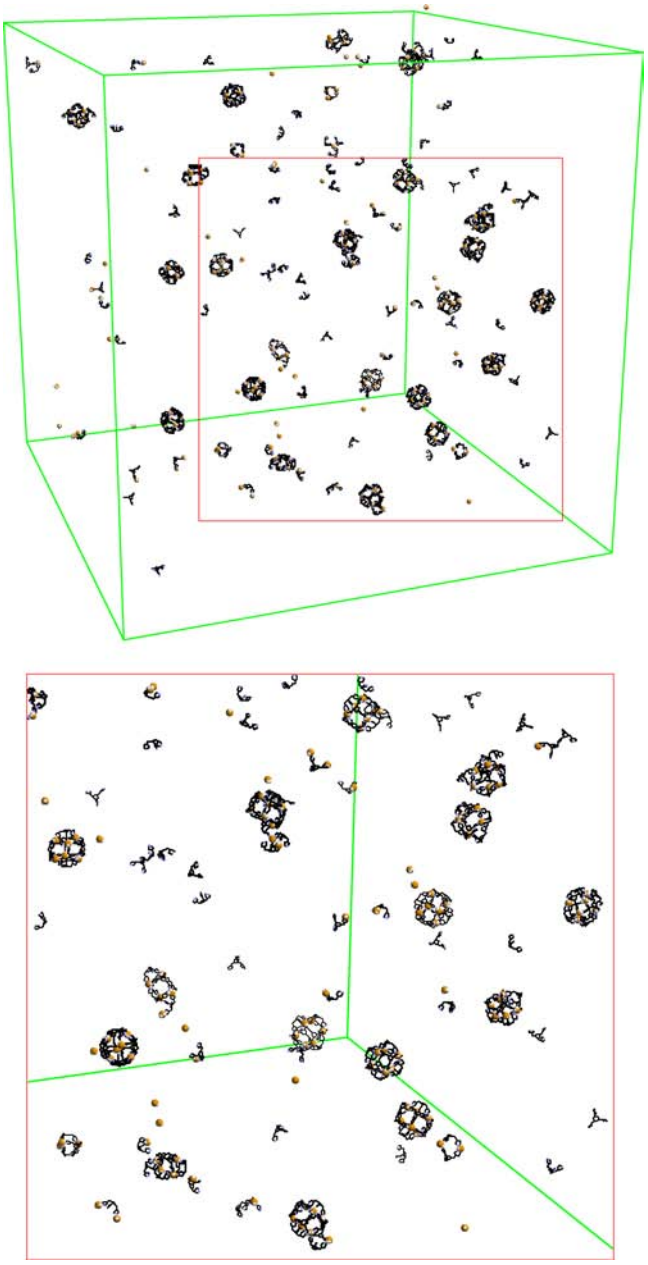

Figure 8. Snapshots after 1 μs LD runs correspond to the case in Figure 7b, i.e., with the forced breakup of the smaller-sized clusters. In this figure, the number of the completed M_6L_8 nanospheres was 17, compared to 32 in a perfect assembly. An enlarged image of the square window part is shown in the below.

The result above corresponded well to the findings in the highly simplified model study of the virus capsid growth.[36] In the icosahedral capsid model with 20 capsomers (subunits), lifetimes of a cluster sized <19 were considerably shorter than those of the complete icosahedral shells with proper attraction parameter settings. These characteristics of the size−lifetime relations, which are accomplished by growth reversibility in the assembly process (i.e., the breakup is even more likely than the growth in the smaller-sized clusters), are pointed out as crucial factors of the capsid self-assembly.[36] We found the same importance through much more direct (realistic) modeling than with the capsid model and completely different intersubunit interactions from those in the capsid model.

The correspondence above strongly supports the general importance of the marked lifetime difference and the growth reversibility in supramolecular self-assembly. As a specific feature of the system in this study, we found the crucial importance of the solvent model in the supramolecular self-assembly through metal−ligand coordination interactions. An investigation of a more appropriate solvent model to further improve speedup of the monodisperse nanosphere formation is underway.

■ ASSOCIATED CONTENT

Ⓢ Supporting Information

The GROMACS molecular topology file (topol.top) for the ligand **1**, CaDA Pd(II), and atomistic solvent and nitrate ion models with the atomic charge assignments. This information is available free of charge via the Internet at http://pubs.acs.org.

■ AUTHOR INFORMATION

Corresponding Author

makoto-yoneya@aist.go.jp

Notes

The authors declare no competing financial interest.

■ ACKNOWLEDGMENTS

We would like to thank Dr. Masuhiro Mikami of Advanced Industrial Science and Technology and Dr. Hiroshi Takeuchi of Hokkaido University for their valuable discussions. This work was supported by KAKENHI (Grant-in-Aid for Scientific Research) in the Priority Area "Emergence in Chemistry" from the Ministry of Education, Culture, Sports, Science, and Technology of Japan.

■ REFERENCES

(1) Lehn, J.; Sanders, J. *Supramolecular chemistry: concepts and perspectives*; VCH: Weinheim, Germany, 1995; Vol. *89*.
(2) Chakrabarty, R.; Mukherjee, P.; Stang, P. *Chem. Rev.* **2011**, *111*, 6810−6918.
(3) Tominaga, M.; Suzuki, K.; Kawano, M.; Kusukawa, T.; Ozeki, T.; Sakamoto, S.; Yamaguchi, K.; Fujita, M. *Angew. Chem.* **2004**, *116*, 5739−5743.
(4) Sato, S.; Iida, J.; Suzuki, K.; Kawano, M.; Ozeki, T.; Fujita, M. *Science* **2006**, *313*, 1273.
(5) Li, D.; Zhou, W.; Landskron, K.; Sato, S.; Kiely, C.; Fujita, M.; Liu, T. *Angew. Chem.* **2011**, *123*, 5288−5293.
(6) Zlotnick, A.; Stray, S. *Trends Biotechnol.* **2003**, *21*, 536−542.
(7) Rapaport, D. *Phys. Rev. E* **2004**, *70*, 051905.
(8) Rapaport, D.; Johnson, J.; Skolnick, J. *Comput. Phys. Commun.* **1999**, *121*, 231−235.
(9) Hagan, M.; Chandler, D. *Biophys J.* **2006**, *91*, 42−54.
(10) Nguyen, H.; Reddy, V.; Brooks, C., III *J. Am. Chem. Soc.* **2009**, *131*, 2606−2614.
(11) Johnston, I.; Louis, A.; Doye, J. *J. Phys.: Condens. Matter* **2010**, *22*, 104101.
(12) Chand, D.; Biradha, K.; Fujita, M.; Sakamoto, S.; Yamaguchi, K. *Chem. Commun.* **2002**, 2486−2487.
(13) Sousa, S.; Fernandes, P.; Ramos, M. *Kinet. Dyn.* **2010**, 299−330.
(14) Pang, Y. *J. Mol. Model.* **1999**, *5*, 196−202.
(15) Wang, J.; Wolf, R. M.; Caldwell, J. W.; Kollman, P. A.; Case, D. A. *J. Comput. Chem.* **2004**, *25*, 1157.
(16) Tiberio, G.; Muccioli, L.; Berardi, R.; Zannoni, C. *ChemPhysChem* **2008**, *10*, 125.
(17) Bayly, C. I.; Cieplak, P.; Cornell, W.; Kollman, P. A. *J. Chem. Phys.* **1993**, *97*, 10269.
(18) Frisch, M. J.; Trucks, G. W.; Schlegel, H. B.; Scuseria, G. E.; Robb, M. A.; Cheeseman, J. R.; Montgomery J. A., Jr.; Vreven, T.;

Kudin, K. N.; Burant, J. C.; Millam, J. M.; Iyengar, S. S.; Tomasi, J.; Barone, V.; Mennucci, B.; Cossi, M.; Scalmani, G.; Rega, N.; Petersson, G. A.; Nakatsuji, H.; Hada, M.; Ehara, M.; Toyota, K.; Fukuda, R.; Hasegawa, J.; Ishida, M.; Nakajima, T.; Honda, Y.; Kitao, O.; Nakai, H.; Klene, M.; Li, X.; Knox, J. E.; Hratchian, H. P.; Cross, J. B.; Bakken, V.; Adamo, C.; Jaramillo, J.; Gomperts, R.; Stratmann, R. E.; Yazyev, O.; Austin, A. J.; Cammi, R.; Pomelli, C.; Ochterski, J. W.; Ayala, P. Y.; Morokuma, K.; Voth, G. A.; Salvador, P.; Dannenberg, J. J.; Zakrzewski, V. G.; Dapprich, S.; Daniels, A. D.; Strain, M. C.; Farkas, O.; Malick, D. K.; Rabuck, A. D.; Raghavachari, K.; Foresman, J. B.; Ortiz, J. V.; Cui, Q.; Baboul, A. G.; Clifford, S.; Cioslowski, J.; Stefanov, B. B.; Liu, G.; Liashenko, A.; Piskorz, P.; Komaromi, I.; Martin, R. L.; Fox, D. J.; Keith, T.; Al-Laham, M. A.; Peng, C. Y.; Nanayakkara, A.; ;, Challacombe, M.; ; W., P. M.; Johnson, B.; Chen, W.; Wong, M. W.; Gonzalez, C.; Pople, J. A. *Gaussian03*, revision C.02; Gaussian, Inc.: Wallingford, CT, 2004.

(19) Smith, P.; Pettitt, B. *J. Phys. Chem.* **1994**, *98*, 9700−9711.

(20) Yun-yu, S.; Lu, W.; Van Gunsteren, W. *Mol. Simul.* **1988**, *1*, 369−383.

(21) Tironi, I.; Sperb, R.; Smith, P.; van Gunsteren, W. *J. Chem. Phys.* **1995**, *102*, 5451.

(22) Weeks, J.; Chandler, D.; Andersen, H. *J. Chem. Phys.* **1971**, *54*, 5237.

(23) Hess, B.; Holm, C.; van der Vegt, N. *Phys. Rev. Lett.* **2006**, *96*, 147801.

(24) Calligaris, M.; Zangrando, E.; Milani, B.; Marson, A. *Eur. J. Inorg. Chem.* **2005**, *2005*, 704−712.

(25) Hess, B.; Kutzner, C.; Van Der Spoel, D.; Lindahl, E. *J. Chem. Theory Comput.* **2008**, *4*, 435−447.

(26) Van Gunsteren, W.; Berendsen, H. *Mol. Simul.* **1988**, *1*, 173−185.

(27) Hess, B.; Bekker, H.; Berendsen, H. J. C.; Fraaije, J. G. E. M. *J. Comput. Chem.* **1997**, *18*, 1463.

(28) Lindahl, E.; Hess, B.; van der Spoel, D. *J. Mol. Model.* **2001**, *7*, 306.

(29) Villa, A.; Mark, A.; Saracino, G.; Cosentino, U.; Pitea, D.; Moro, G.; Salmona, M. *J. Phys. Chem. B* **2006**, *110*, 1423−1428.

(30) Sousa da Silva, A. W.; Vranken, W. F.; Laue, E. D. *Manuscript to be submitted.*

(31) Wang, J.; Wang, W.; Kollman, P.; Case, D. *J. Mol. Graphics Modell.* **2006**, *25*, 247−260.

(32) The threshold distance was extended to 50% larger value if the concerning metal−ligand pairing was not altered from the previous time step to suppress the high-frequency (ca., time step) variations.

(33) Sato, S.; Ishido, Y.; Fujita, M. *J. Am. Chem. Soc.* **2009**, *131*, 6064−6065.

(34) Liu, H.; Mueller-Plathe, F.; van Gunsteren, W. *J. Am. Chem. Soc.* **1995**, *117*, 4363−4366.

(35) Thomas, J.; Roeselová, M.; Dang, L.; Tobias, D. *J. Phys. Chem. A* **2007**, *111*, 3091−3098.

(36) Rapaport, D. *Phys. Rev. Lett.* **2008**, *101*, 186101.

(37) In this simulation, we additionally changed the distance parameter for the complete neutralization in the reaction field method from 1.4 to 1.1 nm to make the metal−ligand electrostatic interactions more short ranged.